PINK1-parkin-mediated mitophagy generates stereotyped somatic mosaicism of the mitochondrial genome

Arnaud Ahier, Chuan-Yang Dai, and Steven Zuryn*.

The University of Queensland, Queensland Brain Institute, Clem Jones Centre for Ageing Dementia Research, Brisbane, Australia.
**Corresponding author.*

Abstract

Mitochondria are critical for complex life and are characterized by the presence of their own genome (mtDNA). The mtDNA makeup within each cell is in a constant state of flux through processes of mutation, replication, and degradation, resulting in a mosaic mtDNA landscape that inevitably varies between cells, tissues, and organs within individuals. However, despite the stochastic nature of these processes, mosaic patterns of mtDNA mutations can become stereotyped across the tissues of individuals in both invertebrate and vertebrate species. The mechanisms that determine the non-random spatiotemporal distribution of mtDNA mutations are unknown. We find that PTEN induced putative kinase (PINK1) and the E3 ubiquitin-protein ligase parkin drive the formation of mtDNA heteroplasmy disparity between the major somatic tissue types of *C. elegans*, generating a stereotyped genetic mosaicism of the mitochondrial genomic landscape. PINK1 and parkin are conserved mediators of mitochondrial autophagy (mitophagy), but while PINK1/parkin preferentially direct the removal of mtDNA mutations in neurons, intestinal cells, and hypodermal cells, they act non-selectively in muscle cells to reduce mitochondrial network volume. These data suggest that different cell types use alternative strategies to cope with mtDNA mutations and implicate the nuclear genome encoded PINK1/parkin signalling axis in shaping stereotyped mitochondrial genomic mosaicism across individuals.

Introduction

Mitochondria act as central hubs for cellular bioenergetics, co-factor and macromolecule precursor synthesis, redox balance, Ca^{2+} handling, apoptosis, and immunity (Spinelli and Haigis, 2018; West and Shadel, 2017). These organelles house their own genome (mtDNA), as well as RNA and protein-synthesizing systems that together code and coordinate the

assembly of core subunits of the oxidative phosphorylation (OXPHOS) machinery used to generate the cell's primary energy substrate, ATP. Although mtDNA lesions that perturb OXPHOS assembly can cause devastating metabolic disorders (Gorman et al., 2016), mutations are buffered by the polyploidy of the mitochondrial genome. Hundreds to thousands of mtDNA copies can populate each cell, which can result in a mixture of multiple mtDNA variants within individual cells and organelles (Morris et al., 2017). This state, termed heteroplasmy, and the factors that influence its dynamics are critical determinants for the pathogenesis of rare mitochondrial diseases, and possibly a wide range of common age-onset inflictions, including neurodegeneration, diabetes, and cancer (Hahn and Zuryn, 2018; Stewart and Chinnery, 2015).

At any given time, an interplay between stochastic and deterministic processes influence cellular heteroplasmy (Hahn and Zuryn, 2018). Mitotic segregation, genetic drift, and the competing effects of homeostatic (Gitschlag et al., 2016; Kandul et al., 2016; Lin et al., 2016; Suen et al., 2010; Valenci et al., 2015) and retrograde signalling pathways (Gitschlag et al., 2016; Lin et al., 2016) may contribute to the divergence of heteroplasmy levels between the cells within a tissue, creating heteroplasmy mosaicism. However, there is evidence that specific organs and tissues are prone to accumulating certain mtDNA mutations more than others, leading to a stereotyped pattern of heteroplasmy mosaicism (Ahier et al., 2018; Samuels et al., 2013; Soong et al., 1992; Wang et al., 2001). For example, the caudate, putamen and substantia nigra regions of the brain show an age-dependent increase in the heteroplasmy levels of the mtDNA^{4977} deletion (a mutant genome harbouring a 4,977bp deletion), relative to the rest of the brain (Soong et al., 1992). In the invertebrate *C. elegans*, stereotyped heteroplasmy differences have also been observed. Here, mtDNA molecules harbouring a large deletion accumulate at different heteroplasmy levels in distinct somatic and germ lineages in a reproducible manner (Ahier et al., 2018). However, it is unknown how these non-random patterns mtDNA heteroplasmy between tissues evolves within individuals.

Here, we have determined that cell-type-specific roles for PTEN-induced putative kinase 1 (PINK1) and the E3 ubiquitin-protein ligase parkin generate stereotyped patterns of mtDNA mosaicism across major somatic tissues in *C. elegans*. PINK1 and parkin are conserved mediators of mitochondrial autophagy (mitophagy), a selective form of autophagy that

removes depolarized mitochondria (Palikaras et al., 2018). The defective organelles are decorated with polyubiquitin chains on their outer surface via PINK1 recruitment of parkin, and are subsequently captured by autophagosomes and destroyed following fusion with lysosomes (Harper et al., 2018). We show that mutations in PINK1 and parkin reverse the stereotyped divergence of mtDNA heteroplasmy observed between neuronal, muscle, intestinal, and hypodermal tissue types. Moreover, we reveal that distinct tissue types use unique strategies to manage mtDNA mutations, which may be dependent upon metabolic requirements. Our results provide a mechanistic rationale for stereotyped mtDNA mosaicism in the soma and provide insights into the processes that contribute to the evolving mtDNA landscape within individuals in both healthy and diseased states.

Results and Discussion

In order to determine whether conserved homeostatic mechanisms such as mitophagy shape stereotyped mosaic patterns of somatic mtDNA distribution, we introduced a heteroplasmic variant of mtDNA that harbours a 3.1 kb deletion (*uaDf5*, also called ΔmtDNA) (Tsang and Lemire, 2002) into double-mutant strains with null deletions in the genes PINK1 (*pink-1*) and parkin (*pdr-1*). The *uaDf5* deletion exists in heteroplasmy with wild-type copies of the mtDNA at a level of approximately 60% across populations of animals (Lin et al., 2016; Tsang and Lemire, 2002). We next crossed these triple mutant strains to transgenic animals carrying a *mos1*-mediated single-copy insertion (mosSCI) of *TOMM-20::mKate2::HA* controlled by either a pan-neuronal promoter (*rgef-1p*), intestinal-specific promoter (*ges-1p*), hypodermis (epidermis)-specific promoter (*dpy-7p*), or body wall muscle (BWM)-specific promoter (*myo-3p*). Using this panel of strains, we performed cell-type-specific mitochondrial affinity purification (CS-MAP) (Ahier et al., 2018), allowing comparisons of mtDNA heteroplasmy across major tissue types in animals lacking PINK-1-PDR-1-mediated mitophagy (Figure 1A).

Heteroplasmy in cell-type-specific mitochondria was investigated across very large populations of pooled animals (>10,000 individuals, see methods). This approach enabled population-scale trends to be resolved by overcoming confounding influences that can be introduced by the presence of stochastic inter-individual variations in mosaicism. Mitochondria were purified from both *pink-1(tm1779)*;*pdr-1(gk448)* double-mutant and wild-type backgrounds carrying ΔmtDNA. To accurately quantify ΔmtDNA heteroplasmy levels

from each tissue type, we used a fluorescence multiplex quantitative PCR (qPCR) assay (Ahier et al., 2018). To eliminate the influence of any inter-population variability affecting our analyses, we compared mitochondria purified from each cell type to the total mitochondria (homogenate) from the same samples. In addition, we performed the same experiments in animals in which mitochondria from all cell types were purified using the same CS-MAP technique. In this case, the ubiquitous promoter *etf-3p* was used to drive the expression of a *TOMM-20::mKate2::HA* transgene integrated into the same genomic location as the other transgenes. As expected, ΔmtDNA heteroplasmy levels did not change between total input mitochondria and mitochondria purified from all cells of wild-type and *pink-1(tm1779)*;*pdr-1(gk448)* backgrounds (Figure 1B). This confirmed that deficiencies in PINK-1 and PDR-1 did not influence the CS-MAP procedure.

However, we found that removal of the PINK-1-PDR-1 mitophagy pathway in mitochondria purified from neurons, intestine, and hypodermis resulted in a significant increase in ΔmtDNA heteroplasmy levels (Figure 1B). This suggests that mitophagy operates within these tissues to selectively remove ΔmtDNA molecules. In wild-type animals, mitochondria isolated from neurons and intestinal cells displayed lower levels of heteroplasmy relative to the homogenate. However, inactivating PINK-1-PDR-1-mediated mitophagy completely reversed this trend, suggesting that PINK-1-PDR-1-dependent mitophagy is particularly important in these cell types for maintaining heteroplasmy levels below the average for the whole animal (Figure 1B). Interestingly, we found that removal of *pink-1* and *pdr-1* had no effect on ΔmtDNA heteroplasmy levels in BWM cells, indicating that PINK-1-PDR-1-mediated mitophagy was not utilised in this tissue type for mitochondrial genome quality control (Figure 1B and 1C). Moreover, removal of *pink-1* and *pdr-1* abolished any differences in ΔmtDNA heteroplasmy levels between all of the major tissue types studied (Figure 1D), suggesting that PINK-1-PDR-1-mediated mitophagy acts to drive stereotyped mosaicism of the mitochondrial genome.

Different cell types have distinct functions and therefore have varying energetic demands. The BWM is composed of four quadrants of somatic muscle bundles, each of which consists of 23-24 cells arranged into staggered pairs that stretch longitudinally from the head to the tail of the animal (Gieseler et al., 2017). The coordinated contractile activities of these bundles produce powerful and energetically demanding sinusoidal body bends that drive locomotion.

We therefore hypothesised that BWM cells might avoid mitophagy in combating mtDNA mutations so as to prevent reductions of the mitochondrial network. To test this idea, we analysed the volume of mitochondria in all tissues using three-dimensional reconstruction of fluorescence images acquired from strains carrying *TOMM-20::mKate2::HA* (Figure 2). We found that the presence of ΔmtDNA tended to increase the volume of the mitochondrial network in neurons, intestine, and hypodermis, although significant increases were only observed in hypodermal tissue (Figure 2A-C and 2E-G). Mitochondrial volume remained unchanged in BWM tissue in the presence of ΔmtDNA (Figure 2D and H). However, we found that removal of *pink-1* and *pdr-1* in this background almost tripled the volume of the mitochondrial network in BWM cells (Figure 2Dc and H). This suggests, as previously demonstrated during ageing (Palikaras et al., 2015), that PINK-1-PDR-1-mediated mitophagy controls the mitochondrial density in *C. elegans* BWM cells. However, unlike in other major tissue types, mitophagy does not counteract the presence of deleterious mitochondrial genomes in the muscle. In contrast, whereas PINK-1-PDR-1-mediated mitophagy appeared to preferentially coordinate the removal of ΔmtDNA in the nervous system, intestine, and hypodermis, it did not appear to play a role in shaping mitochondrial volume, which remained unchanged when both *pink-1* and *pdr-1* were removed in ΔmtDNA backgrounds (Figure 2A-C and 2E-G). One possible explanation for this observation is that cells with high energy demand, such as muscle cells, stimulate high amounts of mitochondrial biogenesis that is balanced through mitophagy-mediated removal. As such, under high mitochondrial turnover conditions, mitophagy may fulfil a different primary role and therefore lose selectivity towards the removal of genetically faulty mitochondria. Indeed, we found that mitophagy restricted the mitochondrial networks to almost one third the volume they would otherwise be in BWM cells, a workload that may saturate the mitophagy machinery. A similar role was not observed in the other major tissue types. Moreover, in wild-type backgrounds, BWM cells had the highest ΔmtDNA heteroplasmy levels of any somatic tissue type (Figure 1B), suggesting that mtDNA quality control is, overall, less efficient in muscle.

The *uaDf5* deletion disrupts four genes that encode core subunits of the electron transport chain and as such, ΔmtDNA is insufficient for the assembly of a functional OXPHOS system. Despite this, we found that BWM activity was unperturbed by the presence of ΔmtDNA. Animals carrying ΔmtDNA could still produce sinusoidal body bends under strenuous

conditions (thrashing assay, see materials and methods) at rates comparable to those of their wild-type counterparts, even when genetically bottlenecked to very high heteroplasmy levels (93.39 ± 0.34%) and tested at various ages up to 5-day old adults (Figure 3A). This suggested that BWM cells could effectively compensate for the presence of deleterious mtDNA in order to maintain function over their lifetimes. Recently demonstrated in mouse sperm, one potential mechanism to compensate for deleterious heteroplasmic mtDNA mutations is to increase the copy number of total mitochondrial genomes (Jiang et al., 2017). Although not helping to remove or repair the mutations themselves, energy supplies might be restored if the expression level of mtDNA-encoded components is increased through an indiscriminate elevation in both mutant and wild-type genome copy number. We therefore investigated whether BWM cells responded to the presence of ΔmtDNA by enhancing mtDNA replication. Indeed, we found that in all tissues except hypodermis, the mtDNA copy number per mitochondrion increased in the presence of ΔmtDNA (Figure 3B). However, the largest absolute increase was observed in BWM mitochondria, with almost 2 additional copies of mtDNA in each mitochondrion (Figure 3C). This suggests that BWM mitochondria have a greater capacity to respond to ΔmtDNA by perpetuating a higher overall copy number of mtDNA per mitochondrion, which may act as an alternative mechanism for maintaining cell function in the absence of mitophagy-mediated mtDNA quality control.

Together, our results suggest that major and distinct tissue systems comprising the three primary germ layers manage deleterious mtDNA mutations by differentially adopting mitophagy and mtDNA biogenesis processes (Figure 3D). Moreover, we have determined that stereotyped distribution patterns of mitochondrial genomes harbouring deletions are caused by disparate roles of PINK-1-PDR-1-mediated mitophagy in different cell types. Interestingly, large mtDNA deletions have been shown to follow stereotyped patterns of accumulation in specific regions of the human brain during ageing (Soong et al., 1992). In the context of our findings, it would be interesting to determine whether such changes are the result of alterations in mitophagy processes in these cells. Indeed, the increase in heteroplasmy levels observed following removal of *pink-1* and *pdr-1* was the greatest in the nervous system. This suggests that neurons are heavily reliant upon mitophagy for the surveillance and removal of mtDNA deletions. Accumulating evidence suggests that mtDNA mutations contribute to the progressive nature of age-related neurodegenerative diseases (Stewart and Chinnery, 2015)

and mitophagy itself has also been shown to be disrupted in models of neurodegeneration (Cummins et al., 2018; Ye et al., 2015). Indeed, mutations in both PINK1 (Valente et al., 2004) and parkin (Kitada et al., 1998) cause early-onset Parkinson's disease, suggesting that perturbations to mitophagy promote neurodegeneration, which in light of our results, may be attributable to the nervous system's reliance on mitophagy for quality control of the neuronal mtDNA landscape.

Figures

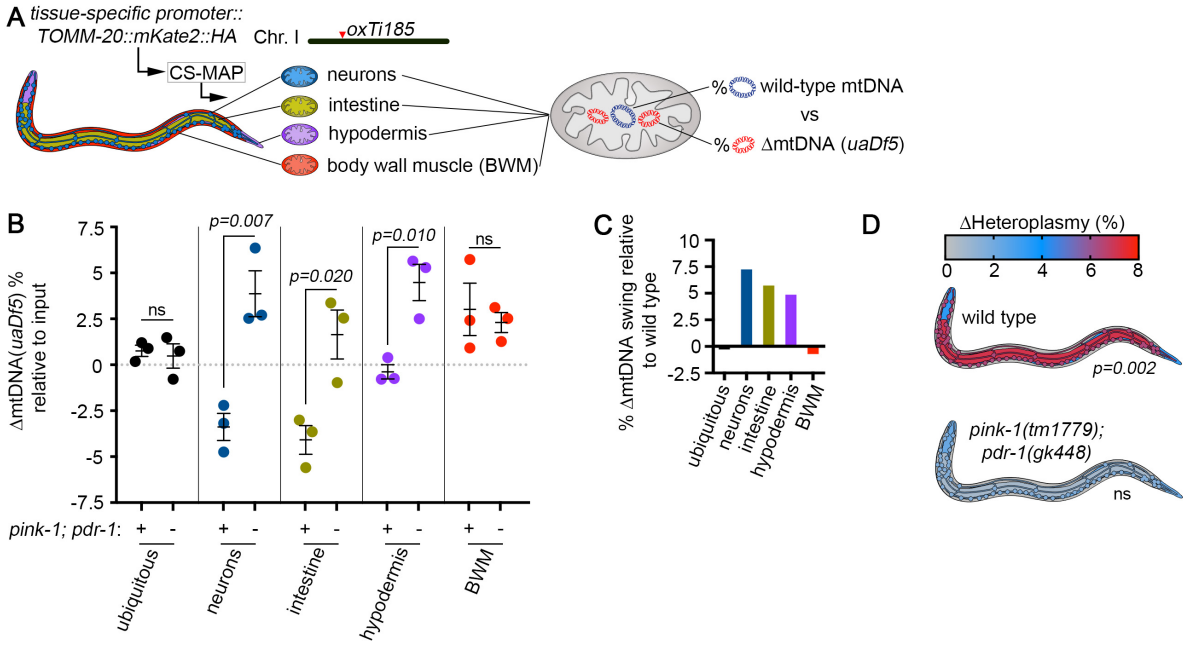

Fig.1 *pink-1* and *pdr-1* determine stereotyped patterns of ΔmtDNA somatic mosaicism. (**A**) Schematic of *C. elegans* and mitochondria originating from major somatic tissue types. *TOMM-20::mKate2::HA* transgenes driven by tissue-specific promoters were integrated into the *oxTi185* site on chromosome 1. In these transgenic animals, cell-specific mitochondrial affinity purification (CS-MAP) was used to purify mitochondria of each cell type from whole animals. Mitochondria harbour both wild-type and ΔmtDNA (*uaDf5*) genomes, a situation known as heteroplasmy. The percentages of each genome were quantified from each sub-population of mitochondria obtained from each cell type. (**B**) Percentage of ΔmtDNA in mitochondria purified from each tissue type, relative to total homogenate. +, animals with functional *pink-1* and *pdr-1* genes; -, animals with deletions in *pink-1* and *pdr-1*. Bars are means ± s.e.m. *P* values were determined using one-way ANOVA and Tukey's correction. (**C**) Summary of the swing in ΔmtDNA % caused by deletion of *pink-1* and *pdr-1* genes, relative to

wild-type animals. (**D**) Graphical representation of the loss of stereotyped inter-tissue variation in ΔmtDNA heteroplasmy in *pink-1;pdr-1* double mutant animals. Each tissue type is coloured according to ΔHeteroplasmy, which is the difference in *uaDf5* heteroplasmy relative to BWM. The significance of heteroplasmy variation between tissues was calculated using one-way ANOVA.

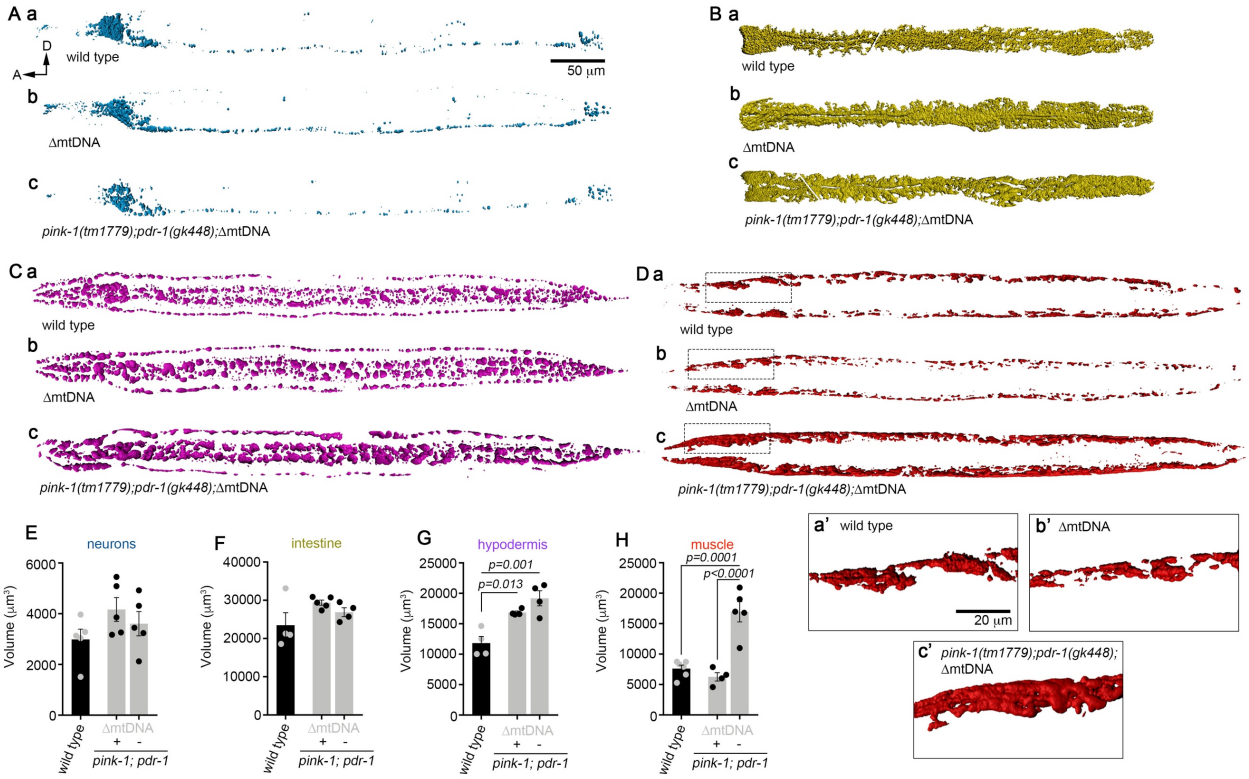

Fig. 2 PINK-1-PDR-1 mediated mitophagy controls mitochondrial network volume in muscle cells. (**A-D**) Representative three-dimensional reconstructions of *C. elegans* (**A**) Complete nervous system mitochondria, (**B**) intestinal mitochondria, (**C**) hypodermal mitochondria, and (**D**) body wall muscle (BWM) mitochondria in (**a**) wild-type animals, (**b**) animals harbouring ΔmtDNA, and (**c**) animals carrying ΔmtDNA in the absence of *pink-1* and *pdr-1* genes (**A-D**, scale bar, 50 μm). For (**D**), dashed boxes are magnified in (**a'-c'**) (scale bar, 20 μm). (**E-H**) Quantification of mitochondrial volumes from each tissue type. Columns are means ± s.e.m. of individual animals (dots). *P* values were determined using one-way ANOVA and Tukey's correction.

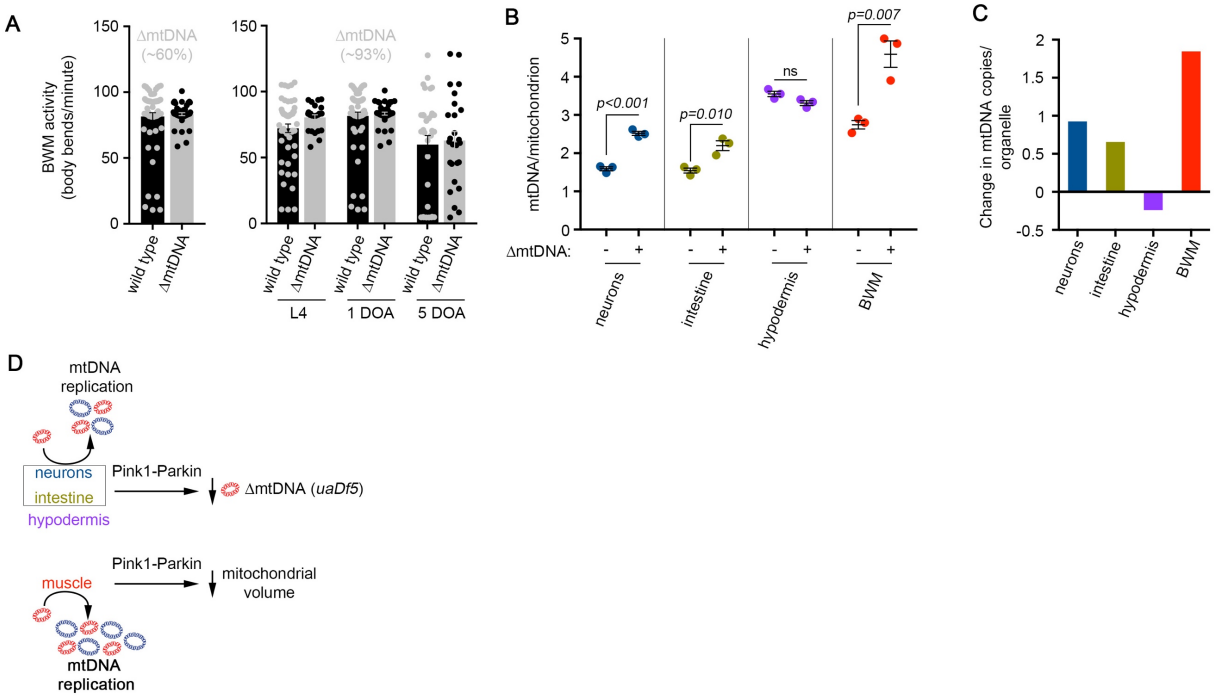

232

233 **Fig. 3 Tissue-specific mtDNA replication in response to the presence of ΔmtDNA.** (**A**)
234 Quantification of body wall muscle (BWM) function using the thrashing assay. ΔmtDNA
235 heteroplasmy levels are shown above each graph. Columns are means ± s.e.m. of individual
236 animals (dots). Two-sided *t*-test. L4, larval stage 4; 1 DOA, 1-day old adult; 5 DOA, 5-day old
237 adult. (**B**) Quantification of mtDNA molecules per mitochondrion (see materials and
238 methods). -, animals not carrying ΔmtDNA; +, animals carrying ΔmtDNA. Bars are means ±
239 s.e.m. *P* values were determined using one-way ANOVA and Tukey's correction. (**C**) Summary
240 of change in mtDNA copy number per mitochondrion caused by the presence of ΔmtDNA,
241 relative to wild-type animals. (**D**) Model summarizing the distinct mechanisms by which
242 different cell types manage mtDNA deletions. Neurons, intestinal cells, and hypodermal cells
243 use PINK-1-Parkin to reduce ΔmtDNA heteroplasmy levels, whereas muscle cells do not. Only
244 neurons, intestinal cells, and muscle cells induce mtDNA replication in response to the
245 presence of ΔmtDNA, with muscle cell mitochondria showing the greatest induction of this
246 response.

247

248 **Materials and Methods**

249 ***C. elegans* strains and culture**. LB138 *him-8(e1489) IV; uaDf5/+*; EG8078 *oxTi185 I; unc-*
250 *119(ed3) III;* BR4006 *pink-1(tm1779) II; byEx655 [pink-1p::pink-1::GFP; myo-2p::mCherry;*
251 *herring sperm DNA]*; VC1024 *pdr-1(gk448) III* and wild-type (N2) were acquired from the

Caenorhabditis Genetics Center (CGC), University of Minnesota, USA, which is funded by the NIH Office of Research Infrastructure Programs (P40 OD010440). *C. elegans* culture and maintenance were performed according to standard protocols (Brenner, 1974). The transgenic strains used for cell-specific mitochondrial purification experiments were generated as previously described (Ahier et al., 2018).

Cell-specific Mitochondrial Affinity Purification (CS-MAP). CS-MAP was performed as previously described (Ahier et al., 2018). Briefly, 10,000 to 20,000 L4 staged worms were grown on 2 x 150 mm NGM plates seeded with *E. coli* OP50 bacteria. Worms were homogenised into a hypotonic buffer [50 mM KCl, 110 mM mannitol, 70 mM sucrose, 0.1 mM EDTA (pH 8.0), 5 mM Tris-HCl (pH 7.4)] with a dounce homogenizer and the subsequent crude mitochondrial fraction was enriched by differential centrifugations and mitochondria were isolated from this fraction using anti-HA (Influenza Hemagglutinin) magnetic beads (Pierce). Beads were washed and resuspended in 20 µl of hypotonic buffer. All CS-MAP experiments were repeated in at least three independent experiments and data for each genetic background were obtained at similar times as previously reported in Ahier et al., 2018 for control wild-type backgrounds.

mtDNA extraction and Quantitative PCR. For all mtDNA analyses, total input and affinity-purified mitochondria were lysed and extracted using phenol-chloroform-isoamyl alcohol, followed by an ethanol precipitation. Extracted DNA was resuspended in 10 mM Tris-HCl (pH 8), 0.1 mM EDTA. Then, multiplex quantitative PCR was performed using the Luna Universal Probe qPCR Master Mix (ref M3004, NEB), a Rotor Gene Q Real-Time PCR (Qiagen) Machine and Rotor Gene Q pure detection software (V2.3.1). The primers 5'-cgtaagaaaatcaaaatatggtataattgg-3', 5'-aaaatgttacgatccttattaataaagc-3', 5'-gcagagatgtttattgaagctgac-3' and the probes 5'-HEX/tgaggccag/ZEN/ttcatattgttccaga gtg/IABKFQ-3' (Iowa Black FQ) and 5'-6-FAM/ccatccgtg/ZEN/ctagaagacaaagaatttc/IABKFQ-3' were used to quantify the wild-type mtDNA and ΔmtDNA levels. Calculations of mtDNA copies per mitochondrion were derived from the quantification of purified organelles in individual samples, as previously performed (Ahier et al., 2018). Control wild-type values are reported in Ahier et al., 2018.

Image acquisition and processing. Imaging was performed on live animals mounted on a 2% agarose pad on glass slides with 1 mM levamisole (Sigma). For quantification of purified mitochondria, we visualized fluorescence using a Zeiss Z2 imager microscope with a Zeiss Axiocam 506 mono camera and Zen2 (version 2.0.0.0) software. Mitochondria were counted with the aid of the Image J Grid plugin, and comparisons were made on the same immunoprecipitation volume for each sample. For 3D reconstruction, images were acquired using a spinning-disk confocal system (Marianas; 3I, Inc.) consisting of an Aanio Observer Z1 (Carl Zeiss) equipped with a CSU-W1 spinning-disk head (Yokogawa Corporation of America), ORCA-Flash4.0 v2 sCMOS camera (Hamamatsu Photonics), 20x 0.8 NA PlanApo and 40x 1.2 NA C-Apo objectives. Image acquisition was performed using SlideBook 6.0 (3I, Inc). 3D reconstruction and mitochondrial volume calculations were performed using 3D rendering in Imaris software (version 8.4.1, Bitplane). Imaging was performed at the Queensland Brain Institute's Advanced Microscopy Facility.

Thrashing assays. Thrashing assays were performed on worms suspended in 40 µl of M9 buffer on a hydrophobic slide (ref G350308BK, ProSciTech). After an initial 3 min period, a 30 second video sequence of the thrashing animals was recorded using a Nikon SMZ745T stereomicroscope and a TrueChrome IIS camera (Tucsen Photonics). Body bends per minutes were determined using CeleST Computer Vision Software as described previously (Restif et al., 2014).

Statistics and Reproducibility. Statistical analyses performed are described for each figure. One-way analysis of variance (ANOVA) was performed for comparisons across multiple independent samples, using Tukey's multiple comparisons correction. All experiments were reproduced at least 3 times with similar results.

Data and reagent availability. All data and biological reagents that support the conclusions of this manuscript are available from the corresponding author on request.

Acknowledgements

We are grateful to R. Tweedale for comments on the manuscript and members of the Zuryn laboratory for discussions and comments. We also thank A. Gaudin for support with

microscopy. Some strains were provided by the CGC, which is funded by the NIH Office of Research Infrastructure Programs (P40 OD010440). This work was supported by NHMRC Project Grants GNT1128381 and GNT1162553, a Stafford Fox Senior Research Fellowship to S.Z., and a University of Queensland International Scholarship to C.Y.D.

Contributions

A.A. carried out most experiments. C.Y.D., S.Z. contributed some experiments. A.A., C.Y.D and S.Z. designed and interpreted experiments and wrote the paper.

Competing Interest

The authors declare that they do not have any financial or non-financial competing interests.

References

Ahier, A., Dai, C.-Y., Tweedie, A., Bezawork-Geleta, A., Kirmes, I., and Zuryn, S. (2018). Affinity purification of cell-specific mitochondria from whole animals resolves patterns of genetic mosaicism. Nat Cell Biol *20*, 352-360.

Brenner, S. (1974). The genetics of Caenorhabditis elegans. Genetics *77*, 71-94.

Cummins, N., Tweedie, A., Zuryn, S., Bertran-Gonzalez, J., and Gotz, J. (2018). Disease-associated tau impairs mitophagy by inhibiting Parkin translocation to mitochondria. EMBO J.

Gieseler, K., Qadota, H., and Benian, G.M. (2017). Development, structure, and maintenance of C. elegans body wall muscle. WormBook *2017*, 1-59.

Gitschlag, B.L., Kirby, C.S., Samuels, D.C., Gangula, R.D., Mallal, S.A., and Patel, M.R. (2016). Homeostatic Responses Regulate Selfish Mitochondrial Genome Dynamics in C. elegans. Cell Metab *24*, 91-103.

Gorman, G.S., Chinnery, P.F., DiMauro, S., Hirano, M., Koga, Y., McFarland, R., Suomalainen, A., Thorburn, D.R., Zeviani, M., and Turnbull, D.M. (2016). Mitochondrial diseases. Nat Rev Dis Primers *2*, 16080.

Hahn, A., and Zuryn, S. (2018). The Cellular Mitochondrial Genome Landscape in Disease. Trends Cell Biol.

Harper, J.W., Ordureau, A., and Heo, J.M. (2018). Building and decoding ubiquitin chains for mitophagy. Nat Rev Mol Cell Biol *19*, 93-108.

Jiang, M., Kauppila, T.E.S., Motori, E., Li, X., Atanassov, I., Folz-Donahue, K., Bonekamp, N.A., Albarran-Gutierrez, S., Stewart, J.B., and Larsson, N.G. (2017). Increased Total mtDNA Copy

Number Cures Male Infertility Despite Unaltered mtDNA Mutation Load. Cell Metab *26*, 429-436 e424.

Kandul, N.P., Zhang, T., Hay, B.A., and Guo, M. (2016). Selective removal of deletion-bearing mitochondrial DNA in heteroplasmic Drosophila. Nat Commun *7*, 13100.

Kitada, T., Asakawa, S., Hattori, N., Matsumine, H., Yamamura, Y., Minoshima, S., Yokochi, M., Mizuno, Y., and Shimizu, N. (1998). Mutations in the parkin gene cause autosomal recessive juvenile parkinsonism. Nature *392*, 605-608.

Lin, Y.F., Schulz, A.M., Pellegrino, M.W., Lu, Y., Shaham, S., and Haynes, C.M. (2016). Maintenance and propagation of a deleterious mitochondrial genome by the mitochondrial unfolded protein response. Nature *533*, 416-419.

Morris, J., Na, Y.J., Zhu, H., Lee, J.H., Giang, H., Ulyanova, A.V., Baltuch, G.H., Brem, S., Chen, H.I., Kung, D.K.*, et al.* (2017). Pervasive within-Mitochondrion Single-Nucleotide Variant Heteroplasmy as Revealed by Single-Mitochondrion Sequencing. Cell Reports *21*, 2706-2713.

Palikaras, K., Lionaki, E., and Tavernarakis, N. (2015). Coordination of mitophagy and mitochondrial biogenesis during ageing in C. elegans. Nature *521*, 525-528.

Palikaras, K., Lionaki, E., and Tavernarakis, N. (2018). Mechanisms of mitophagy in cellular homeostasis, physiology and pathology. Nature Cell Biology *20*, 1013-1022.

Restif, C., Ibanez-Ventoso, C., Vora, M.M., Guo, S.Z., Metaxas, D., and Driscoll, M. (2014). CeleST: Computer vision software for quantitative analysis of C. elegans swim behavior reveals novel features of locomotion. Plos Comp Biol *10*.

Samuels, D.C., Li, C., Li, B., Song, Z., Torstenson, E., Boyd Clay, H., Rokas, A., Thornton-Wells, T.A., Moore, J.H., Hughes, T.M.*, et al.* (2013). Recurrent tissue-specific mtDNA mutations are common in humans. PLoS Genet *9*, e1003929.

Soong, N.W., Hinton, D.R., Cortopassi, G., and Arnheim, N. (1992). Mosaicism for a Specific Somatic Mitochondrial-DNA Mutation in Adult Human Brain. Nature Genetics *2*, 318-323.

Spinelli, J.B., and Haigis, M.C. (2018). The multifaceted contributions of mitochondria to cellular metabolism. Nat Cell Biol *20*, 745-754.

Stewart, J.B., and Chinnery, P.F. (2015). The dynamics of mitochondrial DNA heteroplasmy: implications for human health and disease. Nat Rev Genet *16*, 530-542.

Suen, D.F., Narendra, D.P., Tanaka, A., Manfredi, G., and Youle, R.J. (2010). Parkin overexpression selects against a deleterious mtDNA mutation in heteroplasmic cybrid cells. Proc Natl Acad Sci U S A *107*, 11835-11840.

Tsang, W.Y., and Lemire, B.D. (2002). Stable heteroplasmy but differential inheritance of a large mitochondrial DNA deletion in nematodes. Biochem Cell Biol *80*, 645-654.

385 Valenci, I., Yonai, L., Bar-Yaacov, D., Mishmar, D., and Ben-Zvi, A. (2015). Parkin modulates
386 heteroplasmy of truncated mtDNA in Caenorhabditis elegans. Mitochondrion *20*, 64-70.

387 Valente, E.M., Abou-Sleiman, P.M., Caputo, V., Muqit, M.M., Harvey, K., Gispert, S., Ali, Z.,
388 Del Turco, D., Bentivoglio, A.R., Healy, D.G.*, et al.* (2004). Hereditary early-onset Parkinson's
389 disease caused by mutations in PINK1. Science *304*, 1158-1160.

390 Wang, Y., Michikawa, Y., Mallidis, C., Bai, Y., Woodhouse, L., Yarasheski, K.E., Miller, C.A.,
391 Askanas, V., Engel, W.K., Bhasin, S.*, et al.* (2001). Muscle-specific mutations accumulate with
392 aging in critical human mtDNA control sites for replication. Proc Natl Acad Sci U S A *98*,
393 4022-4027.

394 West, A.P., and Shadel, G.S. (2017). Mitochondrial DNA in innate immune responses and
395 inflammatory pathology. Nat Rev Immunol *17*, 363-375.

396 Ye, X., Sun, X., Starovoytov, V., and Cai, Q. (2015). Parkin-mediated mitophagy in mutant
397 hAPP neurons and Alzheimer's disease patient brains. Hum Mol Genet *24*, 2938-2951.
398